MIGRATION BASED IMAGING USING THE UWB BEAM SUMMATION ALGORITHM

A. Shlivinski(1), **E. Heyman**(2), **K. J. Langenberg**(1)

(1) ***Department of Electrical Engineering, University of Kassel, 34121 Kassel, Germany, samir@uni-kassel.de, langenberg@uni-kassel.de***

(2) ***School of Electrical Engineering, Tel Aviv University, Tel Aviv 69978, Israel, heyman@eng.tau.ac.il***

ABSTRACT

A migration based imaging algorithm is implemented here using the ultra wideband Gaussian beam summation method (UWB-GBS). The image of a scatterer embedded within known background medium is recovered by correlating the backpropagated pulsed scattered wavefield with the forward propagating pulsed field. The forward/backward propagations are performed by decomposing the fields into sets of Gaussian beam (GB) propagators using the UWB-GBS, and the image is formed by generating cross-beam correlation functions (XB-CF) by correlating pairs of forward/backward propagating GB's, and aggregating the products at each image point. Numerical efficiency is gained by using the a-priori beam localization.

INTRODUCTION

Imaging of scatterers embedded in a known medium is an important problem in applications where the scatterers locations rather than their composition are the relevant parameters. Here we form the image by a temporal correlation of the *backpropagated* (migrated) multi bi-static pulsed scattered wave field with the *forward propagation* modelling of the excitation pulsed field. These calculations may be implemented in the frequency domain (FD) or directly in the time domain (TD).

In this work the forward/backward propagation modelling is implemented in the FD by decomposing the fields into a set of Gaussian beam (GB) propagators. As similar approach has been undertaken in [1], but here the analysis is done in the framework of the ultra wideband GB summation method (UWB-GBS) of [2] which provides an *accurate* field modelling using a *sparse, frequency independent* lattice of isodiffracting Gaussian beams (ID-GB, see (7)). The advantages of this approach are: (a) the *same beam set* is used *for all* frequencies; (b) the propagation characteristics of the ID-GB in the ambient environment are calculated only once and then used *for all* frequencies. These properties allow the image to be constructed from aggregating the partial images generated by correlating pairs of forward/backward propagating GB's (cross-beam correlation functions, XB-CF). The XB-CF's are localized in the image domain and may be calculated a priori by frequency domain integration or directly in the time domain.

PROBLEM FORMULATION

The theory is presented in a 2D coordinate frame $\boldsymbol{r}=(x,z)$ with the scatterers residing in the half space $z>0$ that is filled with a known, possibly inhomogeneous, background medium. The excitation is a pulsed aperture source distribution $u_0^i(x;t)$ in the $z=0$ plane and the measured data is the scattered echoes $u_0^s(x;t)$ on the $z=0$ plane at $x\in(x^s_{\min},x^s_{\max})$. The image is created by correlating the backpropagated scattered field $[u^s(\boldsymbol{r};t)]_{\rm bp}$ with the forward propagated source field $u^i(\boldsymbol{r};t)$. Here these operations are performed in the multi-frequency domain, giving

$$\mathcal{I}(\boldsymbol{r})=\int_\Omega d\omega\,[\hat{u}^s(\boldsymbol{r})]_{\rm bp}\left[\hat{u}^i(\boldsymbol{r})\right]^*\,, \tag{1}$$

where $\hat{}$ denotes frequency domain constituents with $e^{-i\omega t}$ time-dependence, Ω is the frequency band of the excitation, and * denotes a complex conjugation. The fields may be defined via the Kirchhoff integrations

$$\hat{u}^i(\boldsymbol{r})=\int dx'\,2\hat{u}_0^i(x')\,\partial_{z'}\hat{G}(\boldsymbol{r},\boldsymbol{r}')\Big|_{z'=0}\,,\quad [\hat{u}^s(\boldsymbol{r})]_{\rm bp}=\int dx'\,2\hat{u}_0^s(x')\partial_{z'}\hat{G}^*(\boldsymbol{r},\boldsymbol{r}')\Big|_{z'=0}\,, \tag{2}$$

where $\hat{G}(\boldsymbol{r},\boldsymbol{r}')$ is the background medium Green's function, and we assumed Dirichlet boundary condition on the $z=0$ plane (similarly it can be used for Neumann boundary conditions). The support of $\mathcal{I}(\boldsymbol{r})$ corresponds to the singular support of the scatterer. The fields propagation in (2) may be carried out with numerous methods. Here we implement them using the UWB-GBS method [2], which is briefly reviewed next.

REVIEW ON UWB-GBS METHOD [2]

The method is formulated within the framework of the theory of overcomplete windowed Fourier transform

(WFT) frames. Assuming a localized window function $\hat{\psi}(x,\omega)$, the WFT frame set is defined as

$$\hat{\psi}_{\boldsymbol{\mu}}(x) = \hat{\psi}(x - x_m)e^{ik\xi_n(x-x_n)}, \qquad \boldsymbol{\mu} = (m,n) = \text{phase space index}, \qquad (x_m,\xi_n) = (m\bar{x}, n\bar{\xi}). \tag{3}$$

The frame elements are localized in the (x,k_x) phase space about the lattice point $(x_m, k\xi_n)$ with $(\bar{x}, k\bar{\xi})$ being the unit cell dimensions. When applied to decompose the source field (see (6)), x_m are the beam initiation points while ξ_n define the beam angles via $\theta_n = \sin^{-1}\xi_n$ for $|\xi_n| < 1$. It is therefore required that the lattice $(\bar{x}, \bar{\xi})$ be frequency independent. In addition, for the set (3) to be overcomplete, the unit cell area $k\bar{x}\bar{\xi}$ must be smaller than 2π. To accommodate these requirements we choose a reference frequency $\bar{\omega} > \omega_{\max} =$ the upper frequency of the excitation source, and require that the lattice be complete at $\bar{\omega}$, i.e., $\bar{k}\bar{\xi}\bar{x} = 2\pi$ where $\bar{k} = \bar{\omega}/c$. This implies that for all $\omega < \bar{\omega}$

$$k\bar{\xi}\bar{x} = 2\pi\nu < 2\pi, \qquad \text{where } \nu(\omega) = \omega/\bar{\omega} = \text{overcompleteness parameter}, \quad \nu < 1. \tag{4}$$

Thus, *scaling the overcompleteness with ω as in* (4) *generates a frequency independent beam lattice.* The aperture-source field $\hat{u}_0^i(x,\omega)$ may be decomposed now for all $\omega < \bar{\omega}$ via

$$\hat{u}_0^i(x) = \sum_{\boldsymbol{\mu}} \hat{a}^i_{\boldsymbol{\mu}} \hat{\psi}_{\boldsymbol{\mu}}(x), \quad \text{with} \quad \hat{a}^i_{\boldsymbol{\mu}} = \langle \hat{u}_0^i(x), \hat{\varphi}_{\boldsymbol{\mu}}(x)\rangle = \int dx\, \hat{u}_0^i(x)\hat{\varphi}^*_{\boldsymbol{\mu}}(x). \tag{5}$$

The expansion coefficients are calculated by projecting the data onto the "dual set" $\hat{\varphi}_{\boldsymbol{\mu}}(x)$ that has the same form as the set $\hat{\psi}_{\boldsymbol{\mu}}(x)$ in (3) but with the window $\hat{\psi}(x)$ replaced by the dual window $\hat{\varphi}(x)$. In general, $\hat{\varphi}$ needs to be calculated for each ω by inverting the "frame operator" associated with $\hat{\psi}$, but if ν is sufficiently small then $\hat{\varphi} \simeq (\nu/\|\hat{\psi}\|^2)\hat{\psi}$. We therefore use $\bar{\omega} \simeq 3\omega_{\max}$ which, following (4), yields $\nu(\omega) < \frac{1}{3}$ for all $\omega < \omega_{\max}$ as required. A smaller $\bar{\omega}$ reduces the redundancy ν^{-1} and thus improves the expansion's efficacy, but on the other hand it hampers its simplicity since $\hat{\varphi}(x)$ needs to be calculated numerically for each ω.

The aperture field representation in (5) can be propagated into the half space $z > 0$ giving

$$\hat{u}^i(\boldsymbol{r}) = \sum_{\boldsymbol{\mu}} \hat{a}^i_{\boldsymbol{\mu}} \hat{B}_{\boldsymbol{\mu}}(\boldsymbol{r}), \qquad \text{with} \quad \hat{B}_{\boldsymbol{\mu}}(r) = \int dx'\, 2\hat{\psi}_{\boldsymbol{\mu}}(x')\partial_{z'}\hat{G}(\boldsymbol{r},\boldsymbol{r}')|_{z'=0}\,, \tag{6}$$

where $\hat{B}_{\boldsymbol{\mu}}$ are the beam propagators into $z > 0$ corresponding to the source distribution $\hat{\psi}_{\boldsymbol{\mu}}(x)$ on the $z = 0$ plane. For $|\xi_n| < 1$ the beam axes emerge from x_m in the direction $\theta_n = \sin^{-1}\xi_n$ whereas for $|\xi_n| > 1$, $\hat{B}_{\boldsymbol{\mu}}$ decay away from $z = 0$ and are neglected in the summation.

We use the isodiffracting GB (ID-GB) window

$$\hat{\psi}_{\text{ID}}(x) = \exp(-kx^2/2b), \quad \text{where } b > 0 \text{ for } \omega > 0. \tag{7}$$

The width of this window, $W_0 = \sqrt{b/k}$, is scaled with frequency so that the collimation (Rayleigh) distance of the resulting GB is *frequency independent* and equals the parameter b (hence the designation ID). It therefore follows that the propagation parameters of these GB's are *frequency-independent* and need to be calculated only once for all frequencies. Collimated beams are obtained if $kb \gg 1$ for the relevant frequencies. Furthermore, for a given ν a snuggest frame is obtained if $\hat{\psi}$ is *matched* to the lattice such that $\Delta_x/\bar{x} = \Delta_\xi/\bar{\xi}$ where $\Delta_{x,\xi}$ are the spatial/spectral widths of $\hat{\psi}$. Thus $\hat{\psi}_{\text{ID}}$ in (7) is matched to the lattice if

$$b = \bar{x}/\bar{\xi} = \bar{k}\bar{x}^2/2\pi, \quad \Rightarrow \quad \text{yielding the snuggest frame for all } \omega < \bar{\omega}. \tag{8}$$

Recalling the discussion after (5), choosing $\bar{\omega} \simeq 3\omega_{\max}$ allows the use of the small ν approximation $\hat{\varphi}_{\text{ID}} \simeq (\nu/\|\hat{\psi}_{\text{ID}}\|^2)\hat{\psi}_{\text{ID}}$ for all $\omega < \omega_{\max}$. Finally, the propagators $\hat{B}_{\boldsymbol{\mu}}$ obtained by using $\hat{\psi}_{\text{ID}}$ in (6) are the so called ID-GB. Analytic expressions for their UWB propagation in inhomogeneous media or for transmission through curved interfaces are given in [3].

Applying the WFT analysis to the scattered field, we obtain the GBS representation of the backpropagated field

$$\left[\hat{u}^s(\boldsymbol{r})\right]_{\text{bp}} = \sum_{\boldsymbol{\mu}'} \hat{a}^s_{\boldsymbol{\mu}'} \left[\hat{B}_{\boldsymbol{\mu}'}(\boldsymbol{r})\right]_{\text{bp}}, \quad \hat{a}^s_{\boldsymbol{\mu}'} = \langle \hat{u}_0^s(x), \hat{\varphi}_{\boldsymbol{\mu}'}(x)\rangle, \quad \left[\hat{B}_{\boldsymbol{\mu}'}(\boldsymbol{r})\right]_{\text{bp}} = \int dx'\, 2\hat{\psi}_{\boldsymbol{\mu}'}(x')\partial_{z'}\hat{G}^*(\boldsymbol{r},\boldsymbol{r}')|_{z'=0}\,, \tag{9}$$

where the backpropagated beam propagators are related to the forward propagators in (6) via

$$\left[\hat{B}_{\boldsymbol{\mu}'}(\boldsymbol{r})\right]_{\text{bp}} = \left[\hat{B}_{\tilde{\boldsymbol{\mu}}'}(\boldsymbol{r})\right]^*, \qquad \text{with} \quad \boldsymbol{\mu}' = (m',n'), \quad \tilde{\boldsymbol{\mu}}' = (m',-n'). \tag{10}$$

Note that the WFT processing for $\hat{a}^s_{\boldsymbol{\mu}'}$ in (9) extracts the local spectral properties of the field, thereby exciting only the relevant beam backpropagators that locally match the data.

IMAGING ALGORITHM WITH BEAM CONTRIBUTIONS

Inserting (6) and (9) into (1) yields the beam-based image via

$$\mathcal{I}(\boldsymbol{r}) = \sum_{\boldsymbol{\mu},\boldsymbol{\mu}'} \mathcal{I}_{\boldsymbol{\mu},\boldsymbol{\mu}'}(\boldsymbol{r}) \qquad \mathcal{I}_{\boldsymbol{\mu},\boldsymbol{\mu}'}(\boldsymbol{r}) = \int_\Omega d\omega\, \hat{a}^s_{\boldsymbol{\mu}'} \left[\hat{B}_{\boldsymbol{\mu}'}(\boldsymbol{r})\right]_{\rm bp} \left[\hat{a}^i_{\boldsymbol{\mu}} \hat{B}_{\boldsymbol{\mu}}(\boldsymbol{r})\right]^* = \text{XB-CF}. \tag{11}$$

$\mathcal{I}_{\boldsymbol{\mu},\boldsymbol{\mu}'}$ are the cross beam correlation functions, evaluated here in the frequency domain, between pairs of forward/backward propagated beams with indexes $\boldsymbol{\mu}$ and $\boldsymbol{\mu}'$, respectively.

To explore the resolution properties of this imaging scheme we consider an isotropic point scatterer at $\boldsymbol{r}_0$ for which scattered data is $\hat{u}^s_0(x) = \hat{u}^i(\boldsymbol{r}_0)\hat{G}(\boldsymbol{r},\boldsymbol{r}_0)|_{z=0}$. Inserting $\hat{u}^s_0(x)$ into (9), using the small ν approximation for $\hat{\varphi}_{\rm ID}$ (see after (8)) and evaluating the integral asymptotically, yields the phase space coefficients (see also in [4])

$$\hat{a}^s_{\boldsymbol{\mu}'} = \hat{u}^i(\boldsymbol{r}_0)\hat{g}_{\boldsymbol{\mu}'}(\boldsymbol{r}_0), \qquad \hat{g}_{\boldsymbol{\mu}'}(\boldsymbol{r}_0) \equiv \langle G(x,\boldsymbol{r}_0), \hat{\varphi}_{{\rm ID}_{\boldsymbol{\mu}'}}(x)\rangle \simeq \left[i\sqrt{\nu/2}/\bar{x}\bar{k}\cos\theta_n\right] \hat{B}_{\tilde{\boldsymbol{\mu}}'}(\boldsymbol{r}_0). \tag{12}$$

Thus, $\hat{g}_{\boldsymbol{\mu}'}$ is non-negligible only for the phase-space constituents $\boldsymbol{\mu}'$ corresponding to the backpropagated beams $\tilde{\boldsymbol{\mu}}'$ that pass near $\boldsymbol{r}_0$. Thus, the WFT processing of the data extracts the local properties of the scattered field and enhances the phase-space constituents corresponding to the direction of arrival from $\boldsymbol{r}_0$. These constituents reside near the phase-space sub-manifold $\boldsymbol{\mu}'(\boldsymbol{r}_0)$ which relates each observation point x'_m with the local directions of arrival ξ'_n from $\boldsymbol{r}_0$. Note that for multiple scattering points, the scattering data is spectrally rich and involves several directions of arrivals ξ'_n at a given observation point x'_m.

For the special case of an isotropic point scatterer, (11) expresses the point spread function (PSF) as a sum of XB-PSF's

$$\text{PSF} \equiv \mathcal{I}(\boldsymbol{r},\boldsymbol{r}_0) = \sum_{\boldsymbol{\mu},\boldsymbol{\mu}'} \mathcal{I}_{\boldsymbol{\mu},\boldsymbol{\mu}'}(\boldsymbol{r},\boldsymbol{r}_0), \qquad \mathcal{I}_{\boldsymbol{\mu},\boldsymbol{\mu}'}(\boldsymbol{r},\boldsymbol{r}_0) = \int_\Omega d\omega\, \underbrace{\hat{a}^{i*}_{\boldsymbol{\mu}} \hat{u}^i(\boldsymbol{r}_0)\hat{B}^*_{\boldsymbol{\mu}}(\boldsymbol{r})}_{\text{forward}} \underbrace{\hat{g}_{\boldsymbol{\mu}'}(\boldsymbol{r}_0)\hat{B}^*_{\tilde{\boldsymbol{\mu}}'}(\boldsymbol{r})}_{\text{backward}} \equiv \text{XB-PSF} \tag{13}$$

Referring to Fig. 1, the localization in the XB-PSF is generated by the overlap of the "spots" generated by the forward and the backward propagating kernels $\hat{a}^{i*}_{\boldsymbol{\mu}}\hat{u}^i(\boldsymbol{r}_0)\hat{B}^*_{\boldsymbol{\mu}}(\boldsymbol{r})$ and $\hat{g}_{\boldsymbol{\mu}'}(\boldsymbol{r}_0)\hat{B}^*_{\tilde{\boldsymbol{\mu}}'}(\boldsymbol{r})$, respectively. Due to $\hat{g}_{\boldsymbol{\mu}'}(\boldsymbol{r}_0)$ in the latter, the "backpropagation spot" is non-negligible only for backpropagated beams $\tilde{\boldsymbol{\mu}}'$ that pass near $\boldsymbol{r}_0$ (see (12)). This spot is centered on the $\tilde{\boldsymbol{\mu}}'$ propagation trajectory at a range corresponding to $\boldsymbol{r}_0$. Its downrange and cross-range widths are given, respectively, by the excitation pulse length $c(\boldsymbol{r}_0)T$ and by the beamwidth $W_{\tilde{\boldsymbol{\mu}}'}(\boldsymbol{r}_0)$. Likewise, the "forward propagation spot" is centered on the $\boldsymbol{\mu}$ trajectory at a range corresponding to $\boldsymbol{r}_0$, and its downrange and cross-range widths are given, respectively, by $c(\boldsymbol{r}_0)T$ and $W_{\boldsymbol{\mu}}(\boldsymbol{r}_0)$. Thus non-negligible $\mathcal{I}_{\boldsymbol{\mu},\boldsymbol{\mu}'}$ are obtained only if the two spots overlap, i.e., if the $\boldsymbol{\mu}$ and the $\tilde{\boldsymbol{\mu}}'$ beams pass near $\boldsymbol{r}_0$. The summation in (13) may therefore be limited, a priori, for $\boldsymbol{\mu} \approx \boldsymbol{\mu}_0(\boldsymbol{r}_0)$ and $\boldsymbol{\mu}' \approx \boldsymbol{\mu}'_0(\boldsymbol{r}_0)$ as defined after (12). Typically, the summation involves only beams passing within the three-beamwidths vicinity of $\boldsymbol{r}_0$ [2].

In the discussion so far we have emphasized the role of the individual XB-CF and its XB-PSF manifestation, but not the role of the excitation which is included implicitly in the coefficients $\hat{a}^i_{\boldsymbol{\mu}}$. Several classes of excitation configurations should be considered. If the source excites only a single collimated beam, say $\check{\boldsymbol{\mu}}$, then the imaging of points $\boldsymbol{r}_0$ along the $\check{\boldsymbol{\mu}}$ is obtained from backpropagated beams $\boldsymbol{\mu}' \approx \boldsymbol{\mu}'_0(\boldsymbol{r}_0)$ as defined above. From Fig. 1 it follows that a localized image with relatively few $\tilde{\boldsymbol{\mu}}'$ is obtained if their backpropagation trajectories are essentially orthogonal to that of $\check{\boldsymbol{\mu}}$. A better coverage of the medium is provided by sources with a wider spectral spread, such as point sources or other distributed source configurations. For a point source excitation, for example, the $\boldsymbol{\mu}$ summation involves essentially a fan of all ξ_n beam-directions emerging from the given source point x_s, but as discussed above, for a given image point $\boldsymbol{r}_0$ this summation may be restricted to $\xi_n \approx \xi_{n_0}(\boldsymbol{r}_0)$.

EXAMPLES

The following examples explores the properties of the algorithm and the effect of the expansion parameters. We consider a homogeneous background with $c=1$, and a point scatterer at $\boldsymbol{r}_0 = (0, 970)$. The excitation is a pulsed ID-GB corresponding to the aperture distribution $\hat{f}(\omega)\exp\{-kx^2/2\alpha\}$ (cf. (7)) where $\hat{f}(\omega)$ represents a modulated Gaussian with center frequency $w_0 = 0.2$ and pulse width $T \sim 57$ (i.e., $\Omega = (0.05, 0.35)$). The parameter α is the collimation distance of the radiated field. We consider three cases: $\alpha = 10$, 700, and 50000. The effective widths of the respective aperture distributions at ω_0 are $\sim \sqrt{\alpha/k_0} \simeq 7$, 60, and 500. The case $\alpha = 10$ is essentially like a point source with a wide radiation pattern, whereas $\alpha = 50000$ yields a wide GB that behaves in the measurement domain almost like a plane wave. The case $\alpha = 700$ represents a physical beam-type transducer with collimation distance 700 and diffraction angle $\sim \sqrt{1/\alpha k_0} \approx 0.08$ radians.

In the beam processing we expanded the source using the ID-GB window (7) with $b = 700$ and $\bar{k} = 1$, so that from (8) $(\bar{x}, \bar{\xi}) \simeq (66.3, 0.095)$ (another option is to express the excitation as a single beam without expanding

it further into beams; see discussion after (13)). The phase-space maps of the expansion coefficients $\hat{a}^i_{\boldsymbol{\mu}}$ for the three cases are shown in Figs. 2(a)– 2(c). One readily observes that for $\alpha = 10$ the source excite a wide spectrum of beams, all emerging essentially from $x_m \approx 0$, while for $\alpha = 50000$ the source excite beams that emerge essentially normal to the aperture ($\xi_n \approx 0$) and from many lattice points x_m.

The expansion coefficients of the scattered field $\hat{a}^s_{\boldsymbol{\mu}'}$ for a point scatterer at $\boldsymbol{r}_0$ are depicted in Fig. 2(d) (from (12) it follows that this phase space distribution is independent of α up to a normalization constant). Recalling (12), non-negligible coefficients reside near the "geometric observation line" [2], which is the phase-space sub-manifold $\boldsymbol{\mu}'(\boldsymbol{r}_0)$ relating the observation points x'_m with the local directions of arrival ξ'_n from $\boldsymbol{r}_0$.

Next, Figs. 3(a)–3(c) depict the XB-PSF footprint (13) for one "forward propagating" beam $\boldsymbol{\mu} = (0,0)$ with three representative "back propagating" beams $\boldsymbol{\mu}' = (0,0)$, $(6,4)$, and $(13,7)$, corresponding to beams that are launched from the measurement plane points $x_m = 0$, 398, and 862 and pass near $\boldsymbol{r}_0$. Note the different footprint size and orientation as implied by the backward beam orientation. Figure 3(d)–3(e) depict the PSF for two aggregation schemes both involving beams from the spatial aperture $|x_{m,m'}| \leq 1500$. In Fig. 3(d) we used the full beam spectrum $|\xi_{n,n'}| \leq 1$ whereas in Fig. 3(e) we used a truncated spectrum $|\xi_{n,n'}| \leq \frac{1}{2}$ (corresponding to a $\pm 30°$ angular propagation sector). The two images are centered at $\boldsymbol{r}_0$, but the spot size of the "truncated" PSF (Fig. 3(e)) is larger since radiation from lattice point with $|x_m| > 560$ has no contribution to the image, and therefore this case is equivalent to an image from a smaller aperture.

REFERENCES

1. N. R. Hill, "Prestack Gaussian-beam depth migration," *Geophysics*, **66**(4), 1240–1250, 2001.
2. A. Shlivinski, E. Heyman, A. Boag, and C. Letrou, "A phase-space beam summation formulation for ultra wideband radiation," *IEEE Trans. Antennas Propagat.*, **52**, 2042–2056, 2004.
3. E. Heyman, "Pulsed beam solutions for propagation and scattering problems," in *Scattering: Scattering and Inverse Scattering in Pure and Applied Science* (R. Pike and P. Sabatier, Eds.), pp. 295–315, Academic Press, 2002.
4. T. Melamed, "Phase-space Greens functions for modeling time-harmonic scattering from smooth inhomogeneous objects", *J. Math. Phys.*, **45**(6), 2232–2247, 2004.

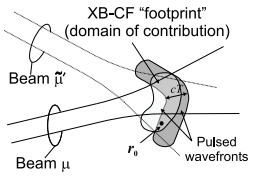

Figure 1: Layout of the cross beam correlation function (XB-CF).

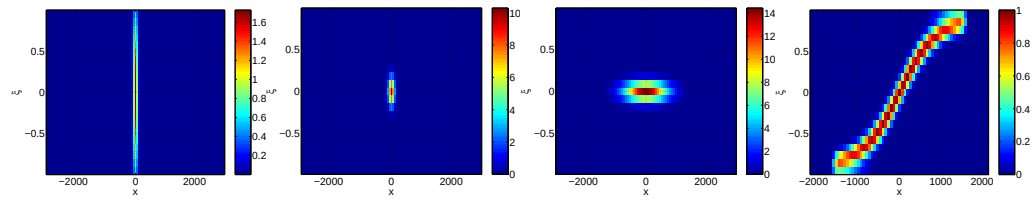

(a) $\hat{a}^i_{\boldsymbol{\mu}}$, $\alpha = 10$ (b) $\hat{a}^i_{\boldsymbol{\mu}}$, $\alpha = 700$ (c) $\hat{a}^i_{\boldsymbol{\mu}}$, $\alpha = 50000$ (d) $\hat{a}^s_{\boldsymbol{\mu}'}$

Figure 2: Maps of the phase-space expansion coefficients at the center frequency ω_0: (a)–(c) the excitation coefficients $\hat{a}^i_{\boldsymbol{\mu}}$ of (5) for the three cases of α; (d) the coefficients $\hat{a}^s_{\boldsymbol{\mu}'}$ of (12) for the scattered field.

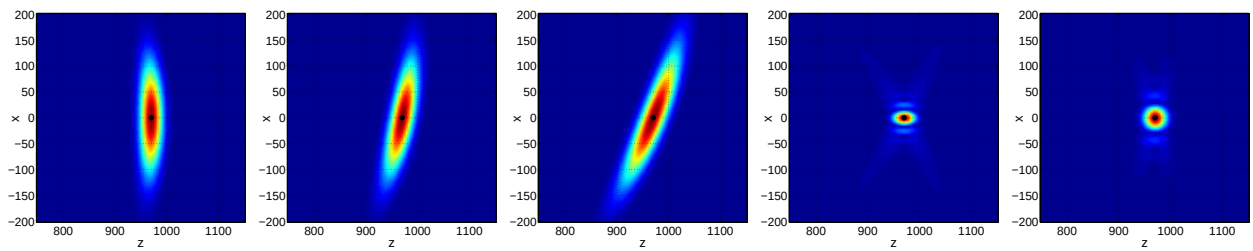

(a) $\boldsymbol{\mu}' = (0,0)$ (b) $\boldsymbol{\mu}' = (6,4)$ (c) $\boldsymbol{\mu}' = (13,7)$ (d) |PSF|: $|\boldsymbol{\xi}_{n,n'}| \leq 1$ (e) |PSF|: $|\boldsymbol{\xi}_{n,n'}| \leq \frac{1}{2}$

Figure 3: The image domain for a point scatterer at $\boldsymbol{r}_0 = (0,970)$ (black dot). (a)–(c) The XB-CF $\mathcal{I}_{\boldsymbol{\mu},\boldsymbol{\mu}'}$ for $\boldsymbol{\mu} = (0,0)$ and for the three $\boldsymbol{\mu}'$ indicated. (d)–(e) The |PSF| obtained by aggregating the XB-CF's of all beams in the visitable range $|\xi_{n,n'}| \leq 1$ (Figure (d)) or over a truncated spectrum of beams $|\xi_{n,n'}| \leq \frac{1}{2}$ (Figure (e)). The colour-map is linear, normalized from zero to the maximum value.